Available online at www.sciencedirect.com
SCIENCE DIRECT®
Journal of Nuclear Materials 334 (2004) 79–89
journal of nuclear materials
www.elsevier.com/locate/jnucmat

Consideration of the effects of partial debonding of the IPyC and particle asphericity on TRISO-coated fuel behavior

Gregory K. Miller *, David A. Petti, John T. Maki

Idaho National Engineering and Environmental Laboratory, P.O. Box 1625, Idaho Falls, ID 83415-3765, USA

Received 26 December 2003; accepted 23 April 2004

Abstract

The fundamental design for a gas-cooled reactor relies on the behavior of the coated particle fuel. The coating layers surrounding the fuel kernels in these spherical particles, consisting of pyrolytic carbon and silicon carbide layers, act as a pressure vessel that retains fission product gases. Many more fuel particles have failed in US irradiations than would be expected when only one-dimensional pressure vessel failures are considered. Post-irradiation examinations indicate that multi-dimensional effects may have contributed to these failures, such as (1) irradiation-induced shrinkage cracks in the inner pyrocarbon (IPyC) layer, (2) partial debonding between the IPyC and SiC layers, and (3) deviations from a perfectly spherical shape. An approach that was used previously to evaluate the effects of irradiation-induced shrinkage cracks is used herein to assess the effects of partial debonding and asphericity. Results of this investigation serve to identify circumstances where these mechanisms may contribute to particle failures.

1. Introduction

The success of gas-cooled reactors depends largely upon the safety and quality of the coated particle fuel. The coating layers of a particle, which surround the fuel kernel and buffer, consist of an inner pyrolytic carbon (IPyC) layer, a silicon carbide (SiC) layer, and an outer pyrocarbon (OPyC) layer. These layers act as a pressure vessel for fission product gases as well as a barrier to the migration of other fission products. The quality of the fuel can be characterized by the number of particle failures that occur during reactor operation. Therefore, a performance model of the coating layers is needed to determine the failure probability of a population of fuel particles. Such a model must account for all viable mechanisms that can lead to particle failure.

The models used to evaluate fuel particles have historically been one-dimensional models (utilizing spherical symmetry) that focus on failures caused by the buildup of internal fission gas pressure. The fuel of the New Production – Modular High Temperature Gas Cooled Reactor (NP-MHTGR) as well as other coated fuel designed in the US has incurred significantly greater levels of failure than are predicted considering just one-dimensional pressure vessel failures, indicating that other mechanisms contributed to failure of the particles. Post-irradiation examinations have revealed the presence of radial shrinkage cracks in the IPyC and OPyC layers, partial debonding between the IPyC and the SiC, and deviations from a spherical shape. To aid in investigating the effects of such multi-dimensional behavior, the Idaho National Engineering and Environmental Laboratory (INEEL) is developing an integrated mechanistic fuel performance code called PARticle FUel ModEl (PARFUME).

Previous studies using this model have shown that shrinkage cracks in the IPyC layer can contribute significantly to the failure of fuel particles [1,2].

* Corresponding author. Tel.: +1-208 526 0360; fax: +1-208 526 4313.
E-mail address: gkm@inel.gov (G.K. Miller).

0022-3115/$ - see front matter © 2004 Elsevier B.V. All rights reserved.
doi:10.1016/j.jnucmat.2004.04.330

Nomenclature

A	aspect ratio for an aspherical particle, or ratio between the major and minor outer diameters for the particle (used to measure the degree of asphericity)
D	standard deviation from the mean value for a parameter that exhibits a particle-to-particle statistical variation
$h(\Delta v)$	function that optimizes the correlation in the calculated maximum stress in a multi-dimensional particle with the stress in a spherical intact particle when parameter v is varied from its mean value
R	outer radius of a TRISO-coated particle μm
r	radius of the facet in an aspherical fuel particle μm
I_n	normalized integration of the stress distribution over the volume of the SiC layer μm^3
m	Weibull modulus for SiC
p	internal gas pressure acting on IPyC layer MPa
σ_c	maximum principal stress in the volume of the SiC layer for a debonded or aspherical particle MPa
σ_u	tangential stress in the SiC layer of an intact spherical particle MPa
$\sigma_{c\bar{v}}$	maximum principal stress in the volume of the SiC layer for a debonded or aspherical particle having all parameters set at mean values for a particle batch MPa
$\sigma_{u\bar{v}}$	tangential stress in the SiC layer of an intact spherical particle having all parameters set at mean values for a particle batch MPa
σ_0	Weibull characteristic strength for the SiC layer MPa $\mu m^{3/m}$
σ_{ms}	effective mean strength for the SiC layer in debonded or aspherical particles MPa
σ_i	$i = 1, 2, 3$, principal stress components in three orthogonal directions MPa
Δv	variation in parameter v from its mean value

PARFUME uses the methodology presented in Ref. [2] to capture the effects of stress concentrations associated with multi-dimensional behavior. That methodology was used here to explore the effects of partial debonding and asphericity on particle failure probability. The results presented serve to identify circumstances where these multi-dimensional effects may contribute to the failure of coated fuel particles.

2. Behavior of the coating layers

The behavior of the three coating layers of the TRISO-coated particle is shown in Fig. 1. Fission gas pressure builds up in the kernel and buffer regions, while the IPyC, SiC, and OPyC act as structural layers to retain this pressure. The IPyC and OPyC layers both shrink and creep during irradiation of the particle while the SiC exhibits only elastic response. A portion of the gas pressure is transmitted through the IPyC layer to the SiC. This pressure generally increases as irradiation of the particle progresses, thereby contributing to a tensile hoop stress in the SiC layer. Countering the effect of the pressure load is the shrinkage of the IPyC and OPyC layers during irradiation, which causes them to push or pull inward on the SiC. Due to anisotropy in the pyrocarbon shrinkage behavior, the shrinkage histories differ in the radial and tangential directions. The shrinkage in the radial direction reverses to swelling at moderate

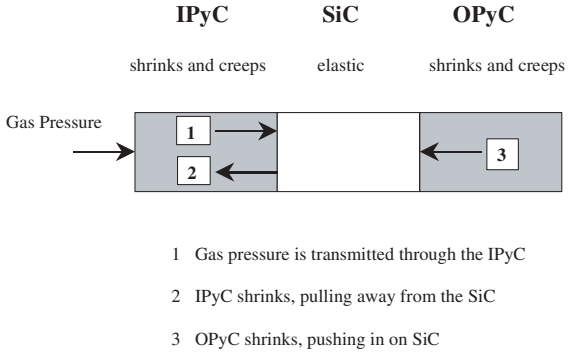

Fig. 1. Behavior of coating layers in a fuel particle.

fluence levels, whereas shrinkage in the tangential direction continues to high fluence levels.

In the stress analyses performed herein, an internal pressure is applied to the IPyC to simulate the fission gas build-up. The shrinkage strain rates and creep coefficients for the pyrocarbons and the elastic properties for the pyrocarbons and the SiC were obtained from data that was compiled in a report by General Atomics in 1993 [3]. As such, the shrinkage strains are treated as functions of four variables, i.e., fluence level, pyrocarbon density, degree of anisotropy (as measured by the Bacon Anisotropy Factor (BAF)), and irradiation temperature. Irradiation-induced creep is treated as secondary creep, with a coefficient that is a function of

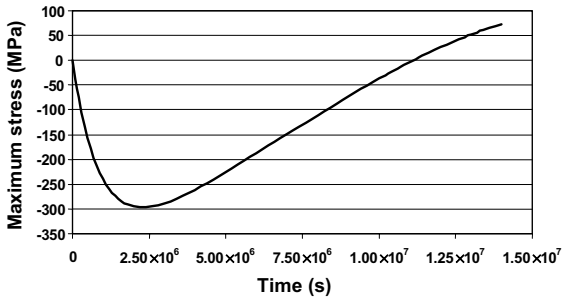

Fig. 2. Tangential SiC stress history for a normal particle.

pyrocarbon density and irradiation temperature. The creep coefficients used in the analyses described herein were set equal to twice the values recommended in the General Atomics data. This is closer to what is used in older performance models [4,5], and has resulted in predictions that are in better agreement with results from irradiation experiments of the New Production – Modular High Temperature Gas Cooled Reactor Program [2]. The elastic modulus for the pyrocarbon layers is applied as a function of four variables (the same variables as used for shrinkage), while the elastic modulus for the SiC is applied as a function of temperature only.

Fig. 2 plots a time evolution for the tangential stress at the inner surface of the SiC layer for a normal spherical particle that is irradiated to a fluence level of 3.5×10^{25} n/m^2 (occurring at a time of 1.4×10^7 s in the analysis). Early during irradiation, the shrinkage of the pyrocarbons layers induces an increasing compressive stress in the SiC. Eventually, creep in the pyrocarbon layers relieves stress in those layers, diminishing the beneficial effect of the shrinkage. Therefore, the tangential stress in the SiC reaches a minimum value, then steadily increases through the remainder of irradiation. A pressure vessel failure has traditionally been expected to occur if the tangential stress reaches a tensile value that exceeds the strength of the SiC for that particle.

3. Methodology

The PARFUME code, which is under development at the Idaho National Engineering and Environmental Laboratory, models the effects of multi-dimensional behavior associated with shrinkage cracking, partial debonding, and asphericity. It utilizes the results of detailed finite element (FE) analyses of cracked, debonded, or aspherical particles in conjunction with results from the one-dimensional (1D) solution described in Ref. [6] to make an approximation of the stress levels in any particle. It is noted that the derivation of the 1D solution has been enhanced in PARFUME in two respects. The first is that it has been extended to allow Poisson's ratio in creep for the pyrocarbons to take on values other than 0.5. Secondly, the solution is applied incrementally such that stresses calculated at the end of an increment become initial conditions for the following increment. This allows material properties, irradiation temperature, and fuel burnup to be varied as desired throughout irradiation.

The statistical approach, as described in Ref. [2], somewhat follows that given in Ref. [7] for treating asphericity in particles, but is more easily applied to other failure mechanisms and is used consistently in PARFUME for all multi-dimensional mechanisms. It allows numerous parameters to be varied statistically (about a mean value), such as thicknesses of the three coating layers, densities and BAF values for the pyrocarbons, irradiation temperature, the creep coefficient for the pyrocarbons, kernel diameter, buffer thickness, and Poisson's ratio in creep for the pyrocarbons. In the approach, FE analyses are performed on just enough cases to determine the effects of varying each parameter individually. The same cases are then analyzed using the 1D solution to calculate stresses in a normal one-dimensional particle. Finally, simple statistical fits are performed on the results of the analyses and a correlation is drawn between the stresses in the one-dimensional and multi-dimensional particles for the same parametric variations.

When several parameters vary statistically about their mean values, as is characteristic of TRISO-coated fuel particles, the maximum principal stress in the SiC layer of the multi-dimensional particle is approximated in PARFUME from:

$$\sigma_c(v_j, v_k, v_l) \cong \frac{\sigma_{c\bar{v}}}{\sigma_{u\bar{v}}}\sigma_u(v_j, v_k, v_l, \ldots)h_j(\Delta v_j)h_k(\Delta v_k)h_l(\Delta v_l)\ldots \tag{1}$$

The quantity Δv_i is the variation of parameter v_i from its mean value for the particles in a batch. Considering all particles in the batch, each variation is characterized by a standard deviation D_i. The stresses $\sigma_{u\bar{v}}$ and $\sigma_{c\bar{v}}$ are the maximum stresses in the SiC layers of the spherical and multi-dimensional particles, respectively, when all parameters v_i are set to their mean values. The latter stress must be determined by performing an FE analysis. The quantities h_i are correlation functions that bring the maximum stress in the spherical particle σ_u into close correlation with the maximum stress in the multi-dimensional particle σ_c. There is a function h_i for every parameter v_i, having the following form:

$$h_i(\Delta v_i) = 1 + c_1\Delta v_i + c_2\Delta v_i^2. \tag{2}$$

The coefficients c_1 and c_2 are determined by performing additional FE analyses, in which the parameter v_i is varied from its mean value, as described in Ref. [2].

A reasonable approximation to the use of Eq. (1) can be attained by dropping some or all of the h functions. If all h functions are dropped, Eq. (1) becomes

$$\sigma_c(v_j, v_k, v_l, \ldots) \cong \frac{\sigma_{c\bar{v}}}{\sigma_{u\bar{v}}}\sigma_u(v_j, v_k, v_l, \ldots). \quad (3)$$

Eq. (3) has the advantage that no FE analyses are required to develop h functions. This is especially useful in performing scoping calculations, where numerous failure probability calculations are required, and a high level of precision is not necessary. In the cases considered in Ref. [2], the error in using Eq. (3) to calculate particle failure probabilities (relative to using Eq. (1)) ranged from 6% to 38%. Because of the large quantity of calculations performed, the approximation of Eq. (3) was used herein to estimate failure probabilities for debonded and aspherical particles.

4. Failure of the SiC

Multi-dimensional behavior generally creates stress concentrations in the SiC material that can lead to particle failure. These stresses are estimated according to the methodology described above and then used to determine particle failure probabilities in the fuel performance model. As has been historically done in fuel particle evaluations, Weibull statistics are used to evaluate failures of the SiC layer. The mean strength for these evaluations is determined from the characteristic strength σ_0 according to the following [2]:

$$\sigma_{\mathrm{ms}} = \sigma_0 / I_n^{1/m}. \quad (4)$$

The characteristic strength for the SiC layer is obtained from the General Atomics data. The integral I_n is a normalized integration of the stress distribution over the volume V of the SiC layer as follows:

$$I_n = \frac{\int_V (\sigma_1^m + \sigma_2^m + \sigma_3^m)\mathrm{d}V}{\sigma_c^m}, \quad (5)$$

where the subscript n denotes a particle having mean values for all parameters. Since only tensile stresses contribute to fracture of the material, compressive stresses are not included in the integration. Whereas Eq. (1) accounts for the magnitude of the maximum stress in the SiC layer, Eq. (5) accounts for the stress distribution in the layer resulting from multi-dimensional behavior.

The integral I_n was calculated for debonded and aspherical particles herein by performing FE analysis using the ABAQUS code [8] on particles having mean values for all statistical parameters. ABAQUS results were transferred to a spreadsheet to perform the integration. The mean strength from Eq. (4) for a batch of fuel particles was then input to PARFUME so that a failure probability could be determined. In the Monte Carlo routine of PARFUME, the maximum stress σ_c in the SiC for each particle was compared to a strength that was sampled from a Weibull distribution having mean strength σ_{ms} and modulus m. Particle failure was then indicated when the maximum stress exceeded the sampled strength.

5. Partial debonding of the IPyC

5.1. Debonding mechanism

Partial debonding between the IPyC and the SiC has been observed in post-irradiation examination (PIE) of the NP-MHTGR fuel particles. During irradiation, shrinkage of the IPyC layer induces a radial tensile stress at the interface between the IPyC and SiC layers. If the stress exceeds the bond strength between layers, then debonding of the IPyC from the SiC occurs. The debonding process is not likely to be an instantaneous detachment over the entire surface of the interface. Rather, it is considered here to begin at an initiation point from which the layers progressively unzip during irradiation. An axisymmetric finite element model for the debonded geometry is shown in Fig. 3. The model plotted is a deformed shape as it appears part way through irradiation, after the unzipping process has begun.

A typical debonded particle was analyzed in a viscoelastic time-integration analysis that progressed until the fluence reached a value of 3×10^{25} n/m^2, occurring at a time of 1.2×10^7 s in the analysis. In the ABAQUS analysis, the IPyC and SiC were initially assumed to be debonded at an arbitrary point in the model. Continued debonding, if it occurred, then progressed from this point. The criterion used was that the node just ahead of the crack tip debonds when the local stress across the interface at a specified distance ahead of the crack tip reaches the specified bond strength. A stress concentration occurs in the SiC layer at the tip of the debonded

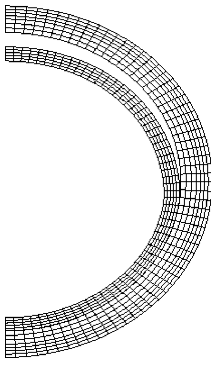

Fig. 3. Finite element model for a partially debonded particle.

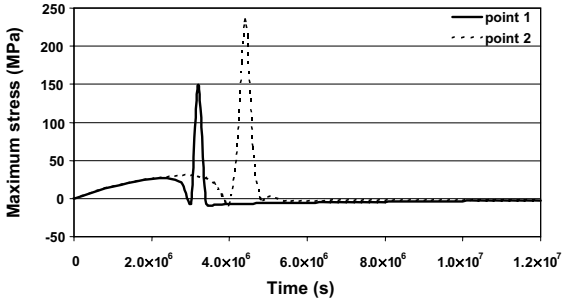

Fig. 4. Inner SiC layer stress histories at two points that experience debonding.

region, containing tensile stress components that could contribute to failure of the SiC. Fig. 4 plots a time history for the maximum calculated principal stress at a point (point 1) on the inner surface of the SiC layer along the debonded path. The stress at this point rose to a peak as the tip of the debonded region passed through this location. With continued unzipping between layers, the stress at this location diminished. Also shown in Fig. 4 is a stress history at a point further down the debonded path (point 2). As would be expected, the stress at this point peaked at a later time during irradiation.

5.2. Particle failure due to debonding

To evaluate particles for potential failure due to debonding, PARFUME first determines whether debonding occurs. It calculates the radial stress at the interface between the IPyC and SiC layers using the closed-form solution described in Ref. [6], and compares this stress to the bond strength between layers. If the code determines that debonding occurs, it then calculates a maximum stress for the SiC layer utilizing the statistical method described above (Eqs. (1) or (3)). Calculations performed herein utilized Eq. (3), which required that only one FE analysis be performed for each batch of particles considered. The code compares this stress to a strength that is sampled from a Weibull distribution having mean strength σ_{ms} and modulus m. The mean strength is calculated from Eq. (4), where the integral I_n represents a stress distribution obtained from the ABAQUS analysis of a debonded particle having mean values for all parameters. With the moving crack tip, significant stress concentrations may occur at numerous points along the debonded path. These stress concentrations are typically not as severe as those at the crack tip of a cracked IPyC, but they occur over a larger portion of the SiC volume. Because the peak stresses at these points do not occur simultaneously, caution must be exercised in calculating I_n to ensure that the stress distribution is based on the maximum stresses that occur at any time during irradiation.

The effects of partial debonding were evaluated by performing failure probability calculations on representative particles assuming a range of values for the bond strength between the IPyC and SiC layers (0–60 MPa). The input parameters for four cases are summarized in Table 1. Each value for the bond strength considered in these calculations was represented by its own batch of particles. Within each batch of particles, the primary statistical variation from particle to particle was a Weibull distribution in the SiC strength. Because the stress distributions in the particle layers change with variations in the bond strength, the Weibull mean strength σ_{ms} from Eq. (4), which is obtained by integrating tensile stresses over the volume of the SiC, is dependent upon the bond strength. Thus, a new value was calculated for σ_{ms} for each bond strength considered. Statistical variations were applied to several of the parameters of Table 1, which had some effect on the calculated failure probabilities.

Results of the debonding calculations are presented in Fig. 5, which shows failure probabilities caused by debonding alone. It is shown that the maximum failure probability for Case 1 occurred when the bond strength

Table 1
Input parameters for debonding calculation

Parameter	Units	Case 1	Case 2	Case 3	Case 4
Kernel diameter	μm	500			
Buffer thickness	μm	100			
IPyC thickness	μm	40			
SiC thickness	μm	35			
OPyC thickness	μm	40			
End-of-life fluence, $E > 0.18$ MeV	10^{25} n/m^2	3.0			
Irradiation temperature	K	973	973	1473	1473
Gas pressure	MPa	4.61	4.61	82.0	82.0
Ambient pressure	MPa	0.1			
IPyC density	10^6 g/m^3	1.90			
OPyC density	10^6 g/m^3	1.90			
IPyC anisotropy	BAF	1.06	1.03	1.06	1.03
OPyC anisotropy	BAF	1.06	1.03	1.06	1.03

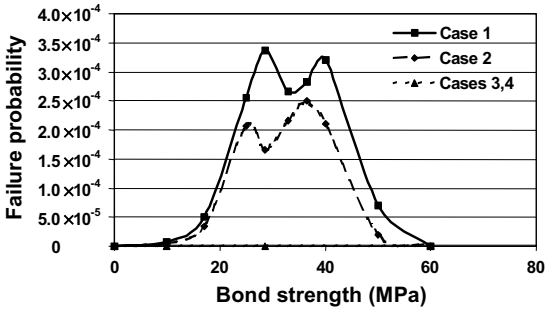

Fig. 5. Failure probability due to debonding as a function of bond strength.

between the IPyC and SiC layers was 28.5 MPa. At very low bond strengths, the IPyC debonded from the SiC layer, but the stress between layers was very small. This resulted in small stresses in the SiC, and consequently low failure probabilities. At large bond strengths (>60 MPa in this case), the radial stress between layers was not sufficient to overcome the bond strength, and there were no failures caused by debonding. In Case 2, the coating layer stresses diminished with a lower anisotropy, and the failure probabilities due to debonding decreased. Because the radial stress between the IPyC and SiC layers decreased with the lower anisotropy, the peaks in the curve also shifted somewhat to lower bond strengths. In this case, the maximum failure probability occurred at a bond strength of 36.5 MPa.

At the higher irradiation temperature of Cases 3 and 4, the radial stress between the IPyC and SiC layers decreased significantly. The effect of an increase in the pyrocarbon shrinkage at the higher temperature was more than offset by the effect of an increase in pyrocarbon creep. The net result was that the higher creep at higher temperature relieved stresses in the coating layers to the point that stresses were not high enough to generate failures due to the debonding process. This result was unaffected by the magnitude of the internal pressure.

The results indicate that a decrease in irradiation temperature increases particle failures caused by debonding of the IPyC. It was previously shown that particle failures caused by cracking of the IPyC also increase with a lower irradiation temperature [1]. In contrast, particle failures associated with the build-up of internal pressure increase with an increase in temperature. This suggests that there may be an optimal intermediate temperature at which the total number of particle failures is a minimum. The optimal temperature for a particular batch of particles is dependent on the values of all the other design parameters, but can in principle be determined by a performance code that integrates all of the failure mechanisms into its failure predictions.

In summary, the debonding calculations show that failures caused by debonding are highly dependent on the irradiation temperature and bond strength. It is noted, however, that there is little data available as to actual bond strengths between the IPyC and SiC. Results also showed that material properties such as anisotropy can have a significant effect on calculated failure probabilities.

5.3. Effect of finite element mesh density

An investigation was made into the effects of changing the finite element mesh density on failure predictions for debonding. The 3×60 finite element mesh shown in Fig. 6 for the SiC layer was modified to a 6×120 mesh, increasing the mesh density by a factor of four. For Case 1 of Table 1 (with a bond strength of 28.5 MPa), this changed the calculated failure probability from 3.37×10^{-4} to 2.80×10^{-4}. The use of a finer mesh increased the calculated maximum stresses in the SiC layer, since the integration points at which stresses were calculated are closer to the crack tip. The finer mesh also resulted in an increased SiC mean strength σ_{ms} from Eq. (4), since the highest calculated stresses occupied a smaller portion of the SiC volume. (The characteristic strength σ_0 is not affected by mesh sizing.) The increase in calculated stress for a finer mesh essentially offset the increase in calculated mean strength, resulting in a small difference in the calculated failure probability. The debonding behavior was sensitive to the specified distance ahead of the crack tip at which debonding was evaluated. The shorter this distance was set, the more readily the IPyC debonded from the SiC. This distance was set to something on the order of the dimension of an element in these analyses, so was shortened for the finer mesh because of the smaller element size.

Results of the analysis indicate that the 3×60 mesh of Fig. 3 is suitable for predicting failures due to debonding. The use of a finer mesh, though also suitable, requires a longer solution time and entails the manipulation of more data to determine the mean strength σ_{ms}.

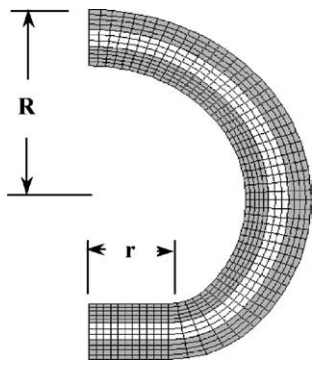

Fig. 6. Finite element model for an aspherical fuel particle.

When a coarser 2×30 mesh was used for the SiC layer, the predicted failure probability decreased by more than an order of magnitude to 1.05×10^{-5}. The maximum calculated stresses decreased, but the mean strength σ_{ms} did not change appreciably. The use of this coarser mesh is not recommended for predicting failures due to debonding.

6. Asphericity

6.1. Behavior of an aspherical particle

Another form of multi-dimensional behavior modeled in PARFUME is asphericity. The program incorporates the effects of asphericity for particles that have a flat facet but that are otherwise spherical. An axisymmetric finite element model for this faceted shape is shown in Fig. 6. A faceted geometry is typical of what has been observed in fabricated particles. Another form of asphericity is an ellipsoidal shape, but this is not characteristic of what has been observed. Furthermore, the effects of an ellipsoidal shape are small relative to the faceted geometry [7]. Therefore, this form of asphericity is not included in PARFUME.

The degree of asphericity for a particle is defined in terms of an aspect ratio, which is the ratio of the major diameter to minor diameter. A reason for defining this parameter is that it is a commonly used measure of the severity of deformity in a particle, and is thereby used as a criterion for particle acceptability. Using dimensions shown in Fig. 6, the aspect ratio (A) is

$$A=\frac{2R}{R+\sqrt{R^2-r^2}}, \tag{6}$$

where R is the outer radius of the particle and r is the radius of the facet.

During irradiation, the faceted portion of the particle acts a flat plate that restrains the internal gas pressure. If the pressure reaches a high enough value, a local region of tensile stress develops in the central portion of the plate that can contribute to particle failures. Unlike failures caused by cracking of the IPyC or partial debonding of the IPyC, which are governed by shrinkage of the pyrocarbons, failures caused by asphericity are dominated by the internal pressure. Therefore, while failures due to IPyC cracking and debonding are predicted to occur early during irradiation when shrinkage stresses are at their highest, failures due to asphericity are likely to occur later when the internal pressure is highest.

A typical faceted particle was analyzed in a viscoelastic time-integration analysis that progressed until the fluence reached a value of 3.5×10^{25} n/m^2, occurring at a time of 1.4×10^7 s in the analysis. Fig. 7 plots a time history for the principal stress in the SiC at the center of the faceted portion of the particle. Also plotted is the corresponding time history for the tangential stress in a spherical particle. A comparison of these stress histories shows that the facet intensifies the stress in that local region of the particle. Depending on its severity, this stress intensification can lead to increased particle failures.

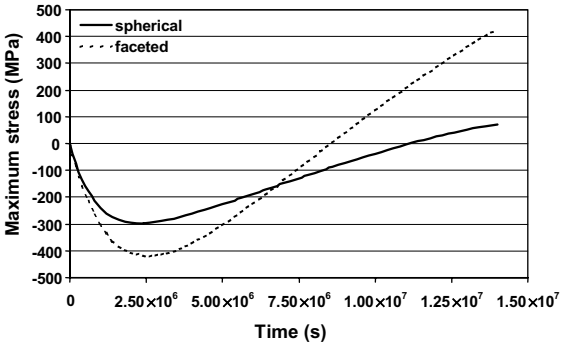

Fig. 7. Stress histories for a faceted and spherical fuel particle.

In evaluating asphericity, PARFUME calculates a maximum stress for the SiC layer utilizing the statistical method described above (Eqs. (1) or (3)). However, a second term is added to correctly estimate the maximum stress σ_c for an aspherical particle. Eq. (3) becomes

$$\sigma_c(v_j,v_k,v_l,\ldots)\cong\frac{\sigma_{c\bar{v}}}{\sigma_{u\bar{v}}}\sigma_u(v_j,v_k,v_l,\ldots)+\frac{\Delta\sigma_{c\bar{v}}}{\Delta\sigma_{u\bar{v}}}\Delta\sigma_u(v_j,v_k,v_l,\ldots), \tag{7}$$

where $\Delta\sigma_{c\bar{v}}$, $\Delta\sigma_{u\bar{v}}$, and $\Delta\sigma_u$ are changes in the stresses $\sigma_{c\bar{v}}$, $\sigma_{u\bar{v}}$, and σ_u in going from the first extremum (or minimum) to the end of irradiation in each respective stress time history. If a second extremum (or maximum) occurs before the end of irradiation is reached, then $\Delta\sigma_{c\bar{v}}$, $\Delta\sigma_{u\bar{v}}$, and $\Delta\sigma_u$ are taken as changes in these stresses in going from the minimum to the maximum. This ensures calculation of the largest value of stress that occurs anytime during the irradiation history. In Eq. (7), $\sigma_{c\bar{v}}$, $\sigma_{u\bar{v}}$, and σ_u are stress values occurring at the time of the minimum in each time history. The first term then takes the solution from time zero to the time of the minimum in the stress history, while the second term takes the solution from the minimum to the end of irradiation or to a maximum, whichever occurs first. The additional term is needed for asphericity evaluations because failures due to asphericity occur after the first extremum for σ_u has been reached, when shrinkage effects from the pyrocarbons are diminishing.

With the addition of a second term, Eq. (1) becomes

$$\sigma_c(v_j,v_k,v_l)\cong\frac{\sigma_{c\bar{v}}}{\sigma_{u\bar{v}}}\sigma_u(v_j,v_k,v_l,\ldots)h_{1j}(\Delta v_j)h_{1k}(\Delta v_k)h_{1l}(\Delta v_l)\cdots+\frac{\Delta\sigma_{c\bar{v}}}{\Delta\sigma_{u\bar{v}}}\Delta\sigma_u(v_j,v_k,v_l,\ldots)h_{2j}(\Delta v_j)\times h_{2k}(\Delta v_k)h_{2l}(\Delta v_l)\cdots \tag{8}$$

The second set of correlation functions h_{2i} is determined in the same way as the first set h_{1i} [2], using output from the same ABAQUS finite element analyses.

Eq. (7) was utilized to perform the calculations described below, since this required that only one ABAQUS finite element analysis be performed for each of the many particle batches considered. There is some question as to how much error is introduced by using Eq. (7) instead of Eq. (8), since these equations include an additional term relative to Eqs. (1) and (3). This is addressed in a representative case presented below.

In these calculations, PARFUME compared the maximum calculated stress (from Eq. (7)) to a strength that is sampled from a Weibull distribution having mean strength σ_{ms} and modulus m. The mean strength is calculated from Eq. (4), where the integral I_n represents a stress distribution obtained from the ABAQUS analysis of a faceted particle having mean values for all parameters.

6.2. Effects of asphericity on NPR-1, HRB-21, and German particles

The effects of asphericity were evaluated by performing failure probability calculations on representative NPR-1, HRB21, and German particles, using the input parameters shown in Table 2. The internal gas pressures shown were calculated using the Redlich–Kwong equation of state [9]. CO production was calculated using algorithms in PARFUME that were produced from computations using the HSC thermochemistry program [10], while fission gas release was calculated using the Booth equivalent sphere model [11] with Turnbull diffusivities [12]. The pressures were calculated in conjunction with a thermal model in PARFUME that computes a temperature profile across the radius of the particle, accounting for a gap that develops between the buffer and IPyC layers.

Failure probability calculations for the three types of particles were performed over a range of aspect ratios. The only statistical variation considered among particles in a batch was a Weibull distribution in strength for the SiC layer. Including statistical variations in other parameters would likely increase the failure probabilities, but the trends should be very similar. Each aspect ratio considered was represented by its own batch of particles. Only failures caused by internal pressure were considered in the calculations, which isolated the effects of asphericity. Because the stress distributions in the particle layers change with variations in the aspect ratio, a new Weibull mean strength was calculated from Eq. (4) for each aspect ratio considered. Results of the calculations are presented in Fig. 8, where it is shown that none of the particles were predicted to fail at very low aspect ratios (a case of zero failures was assigned a probability of 10^{-9} on the logarithmic scale). The HRB-21 particles experienced a significant increase in failure probability at A greater than 1.04. The NPR-1 particles were not affected by asphericity until A reached 1.08, while the German particles showed no propensity to fail at any A value. If the German fuel were operated at the same temperature as the other fuels (1273 K), the calculated internal pressure would increase significantly due to higher CO production predicted by the HSC chemistry model. At this higher pressure, the effects of asphericity would increase the predicted failure rate to 4×10^{-4} at $A = 1.105$, assuming the German fuel to have the same material properties as the other fuel. However, German fuel was produced under different fabrication processes than US fuel, which likely contributed to the superior performance of actual German particles [13].

Table 2
Input parameters for three types of particles

Parameter	Units	NPR-1	HRB-21	German
Kernel diameter	μm	200	351	500
Buffer thickness	μm	102	105	95
IPyC thickness	μm	53	52.8	40
SiC thickness	μm	35	32.6	35
OPyC thickness	μm	39	46.8	40
End-of-life burnup	% FIMA	79	22.5	8.5
End-of-life fluence, $E > 0.18$ MeV	10^{25} n/m^2	3.8	3.5	2.3
Irradiation temperature	K	1260	1273	1173
Internal gas pressure	MPa	18.30	16.81	15.44
Ambient pressure	MPa	0.1	0.1	0.1
IPyC density	10^6 g/m^3	1.923	1.90	1.90
OPyC density	10^6 g/m^3	1.855	1.84	1.90
IPyC anisotropy	BAF	1.0579	1.074	1.04
OPyC anisotropy	BAF	1.0515	1.038	1.04

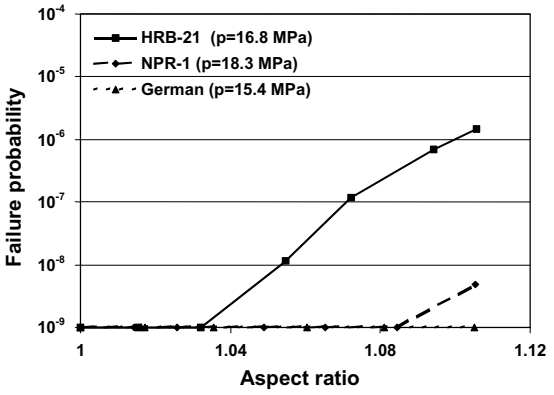

Fig. 8. Failure probabilities as a function of aspect ratio for three types of fuel particles.

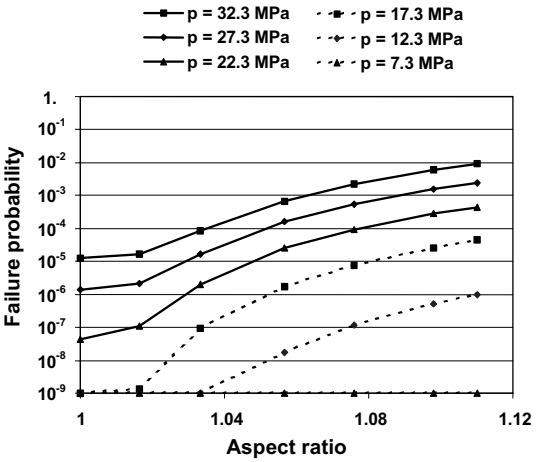

Fig. 9. Failure probability of AGR particles as a function of aspect ratio and gas pressure.

6.3. Effect of asphericity on particles proposed for the DOE Advanced Gas Reactor (AGR) Program

Failure probability calculations were also performed on AGR particles over a range of aspect ratios (1.0–1.11) and internal gas pressures (7.3–32.3 MPa in increments of 5 MPa). The input parameters for these calculations are summarized in Table 3. The material properties in all cases corresponded to an irradiation temperature of 1273 K.

Again, the only statistical variation considered among particles in a batch was a Weibull distribution in strength for the SiC layer. Only failures caused by internal pressure were considered in the calculations, isolating the effects of asphericity. As before, a variation in the Weibull mean strength across the range of aspect ratios was incorporated in the calculations. Results of the calculations are presented in Fig. 9, where it is evident that failures due to asphericity are highly dependent on the pressure and aspect ratio. The failure probability generally increased by several orders of magnitude over the range of 1.0–1.11 in aspect ratio. The high failure probabilities at the higher pressure (32 MPa) suggest that asphericity could be very important under accident conditions.

To aid in visualizing various degrees of asphericity, Fig. 10 presents AGR particle models for A values of 1.0, 1.05, and 1.10. Actual data obtained from measurements of fuel particles from the NPR program showed less than 5% of the particles had $A > 1.12$ (within 95% confidence limits). With improvements to fabrication techniques, lower A values can be expected. Fig. 9 is intended to demonstrate potential effects of asphericity over a range of aspect ratios and pressures, but not to suggest that the performance of actual AGR particles will be adversely affected by asphericity. Calculations of the type that were used to produce Fig. 9 can be used to establish sphericity criteria for the AGR fuel specifications, such that the failure rate associated with asphericity is acceptable.

Table 3
Input parameters for AGR particles

Parameter	Units	Value
Kernel diameter	μm	350
Buffer thickness	μm	100
IPyC thickness	μm	40
SiC thickness	μm	35
OPyC thickness	μm	40
End-of-life fluence, $E > 0.18$ MeV	10^{25} n/m^2	3.5
Irradiation temperature	K	1273
Internal gas pressure	MPa	Varied
Ambient pressure	MPa	0.1
IPyC density	10^6 g/m^3	1.90
OPyC density	10^6 g/m^3	1.85
IPyC anisotropy	BAF	1.03
OPyC anisotropy	BAF	1.03

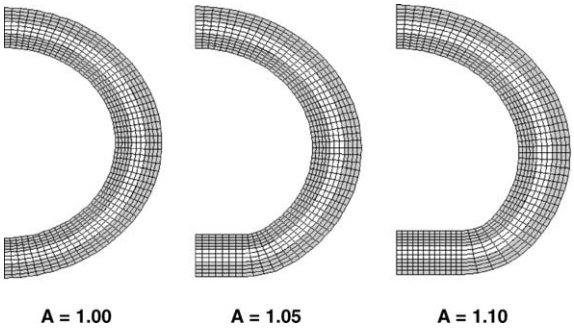

Fig. 10. Finite element models of AGR particles having $A = 1.00$, 1.05, and 1.10.

6.4. Evaluation of error in the use of Eq. (7)

To evaluate the effect on accuracy of using Eq. (7) instead of Eq. (8) in calculating the failure probabilities, further calculations were made for the case of an AGR particle having $A = 1.0567$ and $p = 22.3$ MPa. In this evaluation, the particles were assumed to exhibit Gaussian statistical distributions in the IPyC, SiC, and OPyC thicknesses having standard deviations of 5 μm about the mean values shown in Table 3. With these variations in the layer thicknesses, the use of Eq. (8) yielded a failure probability of 3.56×10^{-5}, while Eq. (7) gave 3.94×10^{-5}. This difference of 11% is within the error range previously experienced when Eq. (3) was used to approximate Eq. (1) for IPyC cracking [2]. The range in values determined for the correlation functions h_{1i} and h_{2i} of Eq. (8) for each of the three parameters, over a range of values that extends four standard deviations to each side of the mean value for that parameter, are listed in Table 4. These are tighter ranges than those determined previously for stresses associated with cracking of the IPyC layer [2]. This means that variations in the stresses in an aspherical particle correlate more closely with variations in stresses in a spherical particle than do stresses in the cracked particle (a perfect correlation would give $h = 1.0$). Therefore, though Eq. (8) is more complex than Eq. (1), the use of Eq. (7) to approximate Eq. (8) for aspherical effects should be of reasonable accuracy.

6.5. Alterations to the faceted geometry

Aspherical effects were represented in the calculations above by a particle having a flat facet with a lead-in radius (Fig. 6) that was sized in proportion to the overall diameter of the particle. Variations to this representation have been observed that could affect the failure probability, such as the size of the lead-in radius or the shape of the faceted portion of the particle. To measure these effects, an AGR particle having $A = 1.0567$ and $p = 22.3$ MPa was evaluated for 1) a 50% increase in the size of the lead-in radius, and 2) a facet that is dimpled inward rather than perfectly flat. Results showed that the larger radius decreased the calculated failure probability from 2.50×10^{-5} to 1.78×10^{-5}, and that the dimpled facet raised the probability from 2.50×10^{-5} to 4.34×10^{-5}. The larger radius somewhat relieved stresses in the faceted region, but did not substantially decrease the failure probability. The dimple decreased stresses in the central portion of the facet but increased stresses in the outer portion, where there is a greater volume of material. While these variations have some effect, the faceted geometry assumed in the study should on balance give a reasonable representation of aspherical effects.

Table 4
Range in values for functions h_1 and h_2

Parameter	h_1	h_2
IPyC thickness	0.94–1.07	0.96–1.06
SiC thickness	0.89–1.00	0.86–1.00
OPyC thickness	0.92–1.06	1.00–1.01

7. Conclusions

The PARFUME code, which is under development at the Idaho National Engineering and Environmental Laboratory, has been used to evaluate the effects of partial debonding (between the IPyC and SiC) and asphericity on the performance of TRISO-coated fuel particles. Results of the studies on debonding indicate that:

- Debonding occurs when the radial stress that develops between the IPyC and SiC layers, due to shrinkage of the IPyC layer, exceeds the bond strength between layers.
- The debonding process is likely to be a progressive unzipping of the two layers that starts at a weak point on the interface between layers.
- Stress concentrations occur at the tip of the debonded region, inducing tensile stress components in the SiC layer that can contribute to particle failures.
- The number of particle failures that occur as a result of debonding is strongly a function of the bond strength between layers. At low bond strengths, the layers readily debond, resulting in low stress in the SiC layer and consequently a low number of failures due to debonding. At a high bond strength, the radial stress between layers may not be sufficient to overcome the bond strength, which again results in a low number of failures due to debonding. Thus, the number of failures due to debonding is greatest at intermediate values for the bond strength.
- The number of failures caused by debonding is also strongly a function of the irradiation temperature. At high temperatures, the creep in the pyrocarbons tends to relax stresses caused by shrinkage, which can in turn greatly reduce the number of failures that would occur due to debonding.
- Material properties such as the anisotropy (as measured by BAF) of the pyrocarbons can also have a measurable effect on the number of failures caused by debonding.

Results of the studies on asphericity indicate that:

- Asphericity is likely to have its greatest effects for particles that have a faceted geometry. The faceted portion of the particle acts as a flat plate that can

incur tensile bending stresses as the gas pressure in a fuel particle builds up, which can contribute to particle failures.

- The number of particle failures caused by asphericity is strongly a function of the internal pressure. The stresses in the faceted portion of a particle are highest when the shrinkage of the pyrocarbons diminishes and the internal gas pressure increases.
- The number of particle failures due to asphericity is also largely dependent on the degree of asphericity, as measured by the aspect ratio for the particle (the ratio between major and minor outer diameters).
- Failure predictions performed on representative fuel particles from the HRB-21 experiment showed that these particles experienced a significant increase in failures (relative to spherical particles) at aspect ratios greater than 1.04, while particles from the NPR-1 experiment showed an increase in failures at aspect ratios greater than 1.08. Meanwhile, predictions for German particles showed no increase in failure probability at any aspect ratio, which was primarily due to a lower irradiation temperature for these particles. Differences in the fabrication process, which were not accounted for here, also affected the performance of actual German particles.
- Predictions made over a range of aspect ratios and gas pressures for representative particles from the proposed AGR program showed that the failure probability typically increased by several orders of magnitude over a range of 1.0–1.11 in aspect ratio. The large failure probabilities predicted for an internal pressure of 32 MPa (ranging up to 10^{-2} at an aspect ratio of 1.11) suggest that asphericity could be very important under accident conditions. Thus, failure predictions that account for the effects of asphericity should be performed to establish sphericity criteria for the specifications for fuel particles that experience high temperatures.

References

[1] G.K. Miller, D.A. Petti, D.J. Varacalle, J.T. Maki, J. Nucl. Mater. 295 (2001) 205.
[2] G.K. Miller, D.A. Petti, D.J. Varacalle, J.T. Maki, J. Nucl. Mater. 317 (2003) 69.
[3] NP-MHTGR Material Models of Pyrocarbon and Pyrolytic Silicon Carbide, CEGA Corporation, CEGA-002820, Rev. 1, July 1993.
[4] J. Kaae, D. Stevens, C. Luby, Nucl. Technol. 10 (1971) 44.
[5] D.G. Martin, Physical and Mechanical Properties of Constituents of Coated Fuel Particles and the Effect of Irradiation, HTR-F WP3 Meeting, Lyon, 2001.
[6] G.K. Miller, R.G. Bennett, J. Nucl. Mater. 206 (1993) 35.
[7] G.K. Miller, D.C. Wadsworth, J. Nucl. Mater. 211 (1994) 57.
[8] ABAQUS User's Manual, Version 6.3, Hibbitt, Karlsson, Sorenson, USA, 2002.
[9] O. Redlich, J.N.S. Kwong, Chem. Rev. 44 (1949) 233.
[10] HSC Chemistry User's Guide, Version 5.0, Outokumpu Research Oy, Finland, 2002.
[11] A.H. Booth, A Method of Calculating Fission Gas Release from UO2 Fuel and its Implication to the X-2-f Loop Test, Atomic Energy of Canada Limited Report – 496, 1957.
[12] J.A. Turnbull et al., J. Nucl. Mater. 107 (1982) 168.
[13] D.A. Petti et al., Nucl. Eng. Des. 222 (2003) 281.